This article has been accepted for publication in a future issue of this journal, but has not been fully edited. Content may change prior to final publication. Citation information: DOI 10.1109/TAP.2020.3017388, IEEE Transactions on Antennas and Propagation

Cavity-Backed Slot-Coupled Patch Antenna Array With Dual Slant Polarization for Millimeter-Wave Base Station Applications

Qingling Yang, Steven Gao, *Fellow, IEEE*, Qi Luo, *Senior Member, IEEE*, Lehu Wen, Yong-Ling Ban, Xuexia Yang, *Senior Member, IEEE*, Xiaofei Ren, and Jian Wu

***Abstract*—This paper presents a novel dual slant polarized antenna for millimeter-wave (mmWave) base stations. Compared with the traditional slant polarized mmWave antennas, the proposed antenna offers the advantages of high cross-polarization discrimination (XPD), good aperture efficiency, simple structure, and low profile. The corner-fed substrate integrated waveguide (SIW) cavity is adopted to improve the port isolation and XPD of this slot-coupled antenna. Four corner-truncated patches connected by a thin cross strip are placed over the SIW cavity to increase the operation bandwidth. Then, a 2×8 antenna array is designed to exemplify the antenna element performance. To improve impedance matching, a shorted patch is introduced in designing the series feeding network and the power divider. The experimental results show that the 2-dB-down gain bandwidth of the proposed antenna array reaches 6.0% and the port isolation is better than 20 dB. The gain and XPD of the antenna array measure 16.7 dBi and 25 dB at the center frequency, respectively.**

***Index Terms*—5G, base station, cavity-backed antenna, dual-polarized antenna, millimeter-wave (mmWave), patch antenna, slant polarization, slot-coupled antenna, SIW cavity**

I. Introduction

BOTH theoretical and experimental results prove that polarization diversity can combat multipath fading, increase channel capacity and improve system reliability [1]–[4]. Polarization diversity also aids in reducing the overall volume and installation cost of the wireless systems. Compared with the horizontally/vertically polarized (HP/VP) antennas, the antennas with $\pm 45^\circ$ dual slant polarization perform better in most scenarios [5], [6]. This is because the received signal strength in HP/VP antenna systems has significant difference whereas the mean signal level in $\pm 45^\circ$ polarized antenna systems is almost equal. During the past two decades, considerable attention has been paid to $\pm 45^\circ$ dual-polarized antennas working in the low frequency bands for 2G/3G/4G base stations [7]–[10] and sub-6 GHz for 5G base stations [11]–[14]. Thanks to the advantages of wide bandwidth, high resolution, high gain, small size, etc., the millimeter-wave (mmWave) technology is considered as one of the potential solutions in future mobile communications for the purpose of delivering gigabits per second (Gb/s) data rate. However, only a few studies on $\pm 45^\circ$ dual slant polarized antenna arrays have been reported for mmWave applications. In [15], a 45° linearly polarized antenna was designed with hollow waveguides, but its configuration is complicated and not suitable for integration. In [16], a microstrip comb-line antenna with matching stubs was proposed to realize 45° slant polarization. However, this antenna suffers from low XPD and narrow bandwidth. Most importantly, these antennas and the 45° inclined slot array antennas reported in [17]–[21] are only able to operate with single slant polarization. Dual polarization can be realized by interleaving the $+45^\circ$ and -45° slant polarized antenna elements as reported in [22]–[24], but it would lead to low XPD, large size and low aperture efficiency. In [25], a mmWave $\pm 45^\circ$ dual-polarized aperture antenna using low-temperature co-fired ceramic (LTCC) technology was proposed to achieve high gain, but this antenna has a very large size ($\approx 2.4\lambda_0 \times 2.4\lambda_0$) which makes it not suitable for the antenna array design. In the low frequency bands lower than 6 GHz, generally speaking, most of the $\pm 45^\circ$ dual-polarized antenna designs for base station applications are inspired by cross dipoles due to their wide bandwidth, high cross-polarization discrimination (XPD), and wide-angle scanning capability [7]–[14]. In [26], a differentially-fed cross slot antenna backed by a SIW cavity is designed to achieve high XPD and good port isolation. However, these antennas cannot be applied to mmWave base stations due to high profile, and high complexity in designing the feeding structures at mmWave frequencies. All of these antennas mentioned above cannot simultaneously meet the requirements of dual slant polarization, high aperture efficiency, small size, low complexity and low profile.

In this paper, a low profile, low complexity and high XPD $\pm 45^\circ$ dual slant polarized cavity-backed slot-coupled patch antenna is developed. To increase the port isolation and XPD, a corner-fed substrate integrated waveguide (SIW) cavity is adopted in the design. The antenna is realized by using four corner-truncated patches connected by a cross strip, which effectively improves the bandwidth without increasing the antenna thickness. The truncated patches are excited by a cross slot. The proposed antenna is different from the

This work was funded by China Research Institute of Radiowave Propagation, Engineering and Physical Sciences Research Council (EPSRC) under grants EP/P015840/1, EP/N032497/1, and EP/S005625/1. (*Corresponding author: Qingling Yang*)

Q. Yang, S. Gao, Q. Luo and L. Wen are with the School of Engineering and Digital Arts, University of Kent, Canterbury CT2 7NZ, UK.

Y. Ban is with the School of Electronic Science and Engineering, University of Electronic Science and Technology of China, Chengdu 611731, China.

X. Yang is with the School of Communication and Information Engineering, Shanghai University, Shanghai 200444, China.

X. Ren and J. Wu are with the China Research Institute of Radiowave Propagation, Xinxiang, Henan 453003, China.

This article has been accepted for publication in a future issue of this journal, but has not been fully edited. Content may change prior to final publication. Citation information: DOI 10.1109/TAP.2020.3017388, IEEE Transactions on Antennas and Propagation

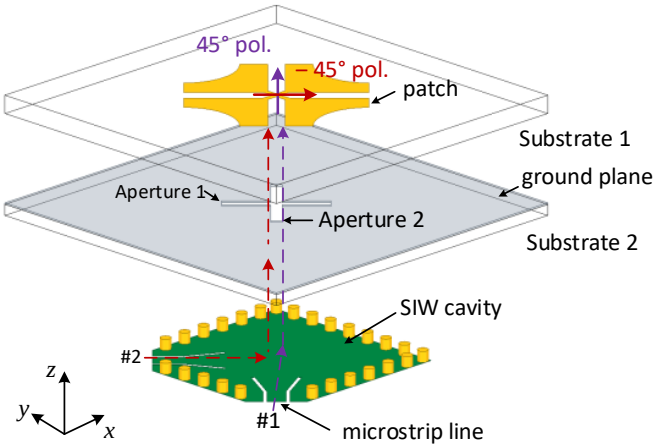

Fig. 1. Geometry of the proposed cavity-backed slot-coupled patch antenna with ±45° dual slant polarization.

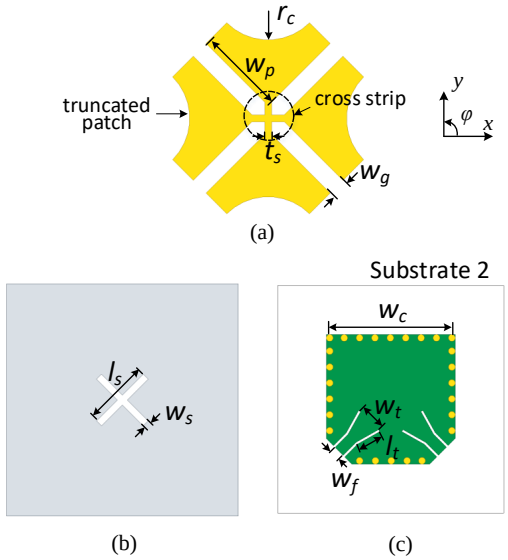

Fig. 2. Top view of each structure in the proposed antenna. (a) Radiating patch. (b) Cross slot etched on the ground plane. (c) SIW cavity in Substrate 2. (Detailed dimensions: $w_p = 2.19$ mm, $w_g = 0.45$ mm, $r_c = 1.46$ mm, $t_s = 0.17$ mm; $l_s = 2.84$ mm, $w_s = 0.3$ mm; $w_c = 5.4$ mm, $w_f = 0.6$ mm, $l_t = 1.1$ mm, $w_t = 1.22$ mm.)

antenna reported in [27] where the bandwidth improvement is achieved by introducing a rectangular loop and increasing the cavity height. To verify the performance of the proposed antenna, a 2×8 antenna array is fabricated and measured. The measurement shows that the developed antenna array has a good performance in terms of impedance bandwidth, port isolation, XPD, aperture efficiency, and radiation patterns.

This paper is organized as follows. The geometry and design of the proposed antenna is presented in Section II. Section III illustrate the design of the antenna array and feeding networks. Section IV gives the simulated and measured results, as well as discussions. A conclusion is given in Section V.

II. Cavity-Backed Slot-Coupled Patch Antenna

A. Geometry

Fig. 1 shows the geometry of the proposed cavity-backed slot-coupled patch antenna. Two Rogers RO4003C laminates with relative dielectric constant $\varepsilon_r = 3.55$ and loss tangent $\tan\delta = 0.0027$ are used in the design. An SIW cavity is built in Substrate 2 and excited at two neighboring corners. Port #1 and #2 are the feeding ports for $+45°$ and $-45°$ slant polarization, respectively. They are designed with microstrip lines printed on the bottom surface of Substrate 2. A cross slot is etched on the ground plane. On the top surface of Substrate 1, two pairs of planar patches are printed. Different from the patch antenna reported in [28] where four separate patches are placed over a slot aperture, the patches in our design are truncated at the corners and a cross strip is added at the center of antenna to connect these patches. It is found that good impedance matching is difficult to obtain when separate patches are excited by a slot aperture in mmWave band frequencies [29]. It will be demonstrated in the following section that the introduced cross connection aids in improving the antenna impedance matching. Considering the bandwidth improvement and surface-wave suppression, Substrate 1 should have a moderate thickness. To avoid using wide microstrips, Substrate 2 is chosen to have a relatively low thickness. Thus, the thickness of Substrate 1 and Substrate 2 is chosen as 0.508 mm and 0.305 mm, respectively. The corner-truncated patch antenna is excited by the cross slot. Aperture 1 positioned along the $\varphi = +45°$ direction couples the signal input from port #1 to excite the patch antenna for $+45°$ slant polarization, while Aperture 2 positioned along the $\varphi = -45°$ direction is used to excite the patch antenna for $-45°$ polarization. Due to the orthogonality between the diagonal TE_{120} and TE_{210} mode inside the SIW cavity, high isolation between port #1 and #2 and high XPD are expected. Detailed dimensions of the proposed antenna are illustrated in Fig. 2.

B. Slot Antenna Designed on Square SIW Cavity

The proposed antenna is developed from a cavity-backed slot antenna, as shown in Fig. 3(a). A cross slot antenna is etched over the cavity and 45° tilted away from the y-axis. The antenna is excited by the inset microstrips at two neighboring corners of the SIW cavity. To illustrate the corner-fed SIW cavity used in the antenna design, another reference model, namely edge-fed cavity-backed slot antenna, is also investigated. As shown in Fig. 3(b), to achieve ±45° dual slant polarization the overall structure of the reference antenna is 45° tilted away from the y-axis [30]. In these two designs, the SIW cavity supporting TE_{120} and TE_{210} modes is used. The resonance frequency of a designated TE_{mnp} mode in a square SIW cavity is given by [31]

$$f_{mnp} = \frac{c}{2\pi\sqrt{\varepsilon_{r,eff}}}\sqrt{\left(\frac{m\pi}{W_{eff}}\right)^2 + \left(\frac{n\pi}{W_{eff}}\right)^2 + \left(\frac{p\pi}{h}\right)^2} \quad (1)$$

where $\varepsilon_{r,eff}$ is the effective dielectric constant of the used laminate. W_{eff} and h are the effective width and thickness

This article has been accepted for publication in a future issue of this journal, but has not been fully edited. Content may change prior to final publication. Citation information: DOI 10.1109/TAP.2020.3017388, IEEE Transactions on Antennas and Propagation

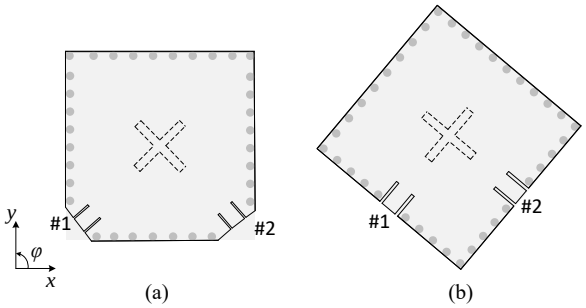

Fig. 3. Slot antenna designed on a square SIW cavity fed from different positions. (a) Corner-fed. (b) Edge-fed.

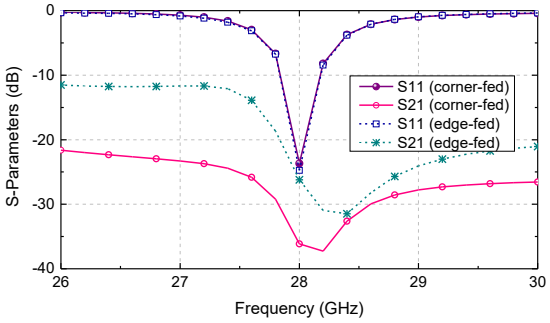

Fig. 4. Simulated *S*-parameters of the corner-fed and edge-fed cavity-backed slot antenna.

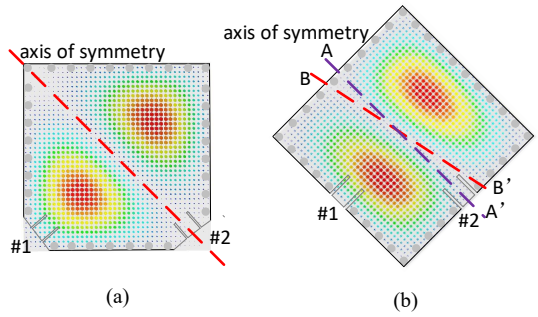

Fig. 5. Diagonal TE_{120} mode field distribution in the square SIW cavity fed from different positions when port #1 is excited. (a) Corner-fed. (b) Edge-fed.

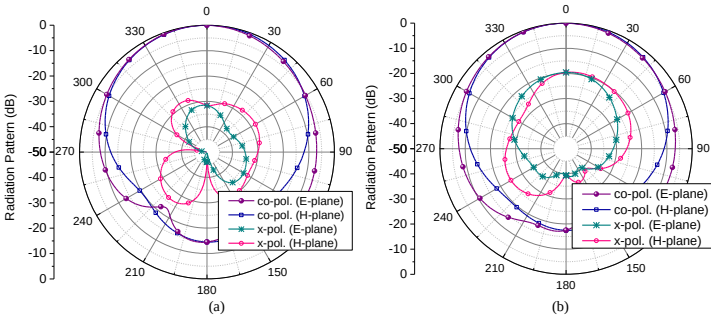

Fig. 6. Normalized radiation patterns of the two slot antennas when port #1 is excited. (a) Corner-fed antenna. (b) Edge-fed antenna.

of the SIW cavity, respectively. An SIW cavity has the same resonance characteristics as a square metallic cavity filled with the same dielectric material. Empirically, an SIW cavity can be considered as a square metallic cavity by using the following equivalence [32]

$$W_{eff} = W - 1.08\frac{d^2}{s} + 0.1\frac{d^2}{W} \tag{2}$$

where W is the physical width of the square metallic cavity filled with the same dielectric material. d and s are the via diameter and spacing between neighboring vias, respectively. By applying (1) and (2), the initial cavity size for designing the two antennas can be obtained.

Fig. 4 shows the simulated *S*-parameters of the two antennas. Although the only difference between the two antennas lies in their feeding positions for dual polarization, the port isolation of the corner-fed cavity-backed slot antenna is much better than that of the edge-fed one. At the center frequency 28 GHz, the isolation between port #1 and #2 of the edge-fed antenna is 26 dB, whereas for the corner-fed antenna the port isolation is 36 dB. The reflection coefficient curves of the two antennas are almost identical. Due to only single mode excited in the cavity and the inherent characteristic of slot antennas, their impedance bandwidth for $|S_{11}| < -10$ dB is quite narrow, which is from 27.8 GHz to 28.2 GHz.

The electric field patterns in the SIW cavities of Fig. 3 are shown in Fig. 5. It is observed that the TE_{120} mode field in the corner-fed cavity is well odd symmetric with respect to the backward diagonal when port #1 is excited, as shown in Fig. 5(a). The electric field is almost null along the diagonal. However, it is found in Fig. 5(b) that the electric field pattern inside the edge-fed cavity is odd symmetric with respect to the reference line BB', but not identical with the ideal TE_{120} field pattern, whose field distribution is odd symmetric with respect to the axis of symmetry AA'. This is primarily resulted from perturbation introduced by the feeding ports. However, perturbation introduced by the ports in the corner-fed cavity is almost negligible since its effective size for the diagonal TE_{120} mode is larger than the size of the edge-fed cavity. It is also demonstrated in [33] that thin substrate would increase perturbation for the modes inside the cavity. As a result, the port isolation between port #1 and #2 of the corner-fed cavity is higher than the port isolation in the edge-fed cavity. Fig. 6 shows the normalized radiation patterns of the two antennas. In this design, the E-plane is defined as the plane of $\varphi = 45°$, and the H-plane is defined as the plane of $\varphi = -45°$. It is observed that the co-polarization patterns of the corner-fed antenna are very similar to the edge-fed antenna since they have the same slot radiating aperture. However, as one of the key parameters in evaluating antenna performance, the XPD of the corner-fed antenna is much lower. The XPD of the corner-fed antenna is 32 dB, whereas the XPD from the edge-fed antenna is only 19 dB. This difference is resulted from the mode misalignment in the edge-fed cavity. Since the TE_{120} mode in the edge-fed cavity is rotated by a certain angle with respected to AA', cross-polarized electric fields are radiated from the slot etched over the cavity.

This article has been accepted for publication in a future issue of this journal, but has not been fully edited. Content may change prior to final publication. Citation information: DOI 10.1109/TAP.2020.3017388, IEEE Transactions on Antennas and Propagation

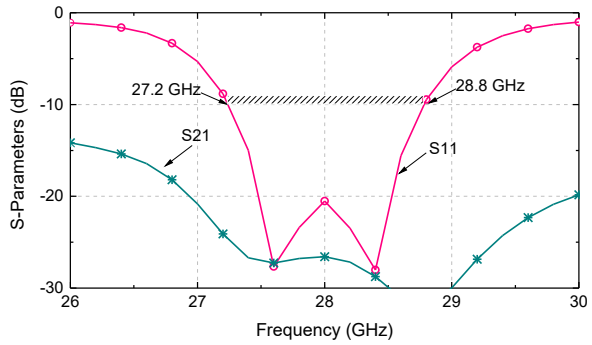

Fig. 7. Simulated *S*-parameters of the proposed antenna.

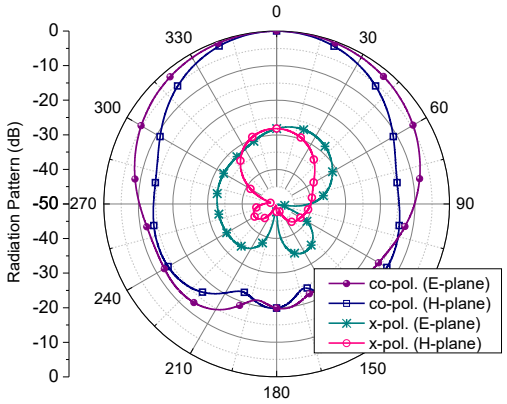

Fig. 8. Radiation patterns of the proposed antenna.

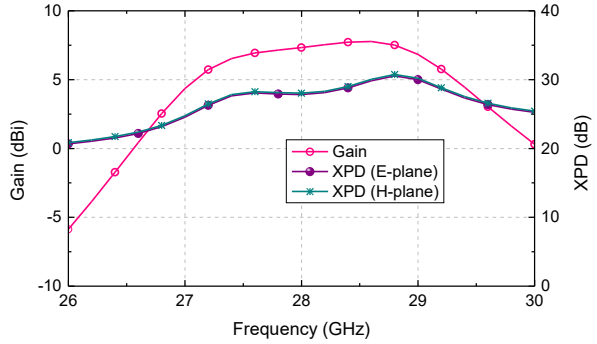

Fig. 9. Simulated gain and XPD versus frequencies.

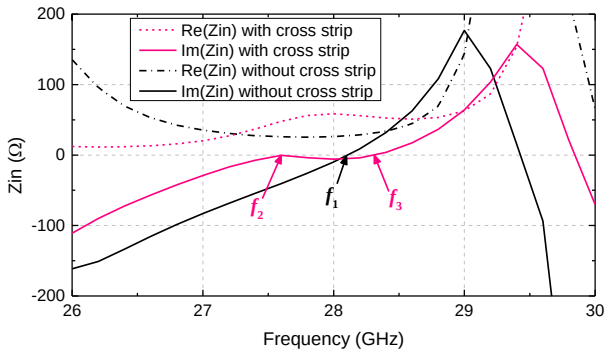

Fig. 10. Simulated *S*-parameters of the proposed antenna and the corresponding antenna without the cross strip.

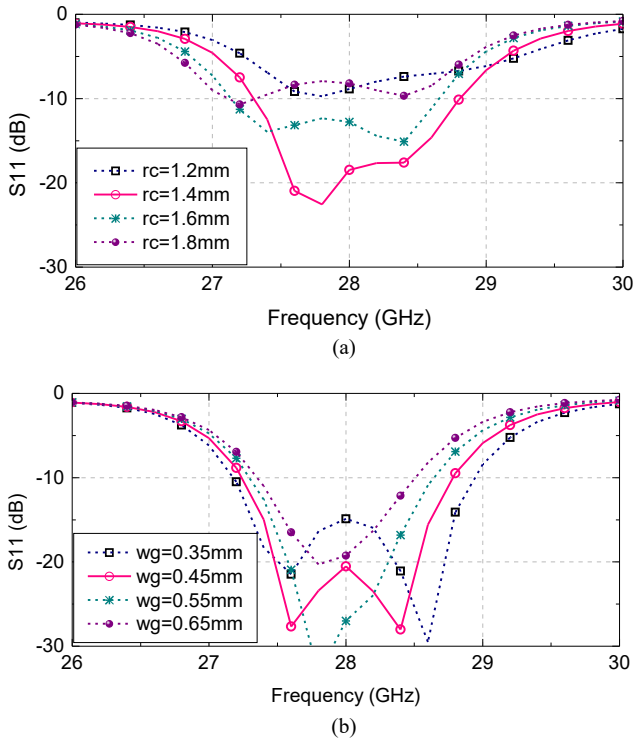

Fig. 11. Simulated $|S_{11}|$ of the proposed antenna. (a) With different truncated corner size (r_c). (b) With different gaps between patches (w_g).

C. Bandwidth Improvement

With odd symmetrical TE_{120} and TE_{210} mode patterns inside the SIW cavity, high isolation (36 dB) and high XPD (32 dB) are achieved in the corner-fed antenna at the center frequency. However, the bandwidth of this antenna is quite narrow, only 400 MHz (27.8-28.2 GHz).

To overcome this problem, four corner-truncated parasitic patches are printed on the top surface of Substrate 1, and they are connected by a thin cross strip, as shown in Fig. 2(a). The simulated performances of the proposed antenna are illustrated from Fig. 7 to Fig. 9. As shown in Fig. 7, two resonances are observed at 27.6 GHz and 28.4 GHz, respectively. The impedance bandwidth for $|S_{11}| < -10$ dB is 1.6 GHz, from 27.2 GHz to 28.8 GHz. Within this frequency band, the isolation between port #1 and #2 is higher than 26.5 dB. The decrease of the port isolation is because the introduction of the patch perturbs the field distribution of the TE_{120} or TE_{210} mode inside the cavity. Fig. 8 presents the radiation patterns of the proposed antenna. Symmetric patterns are observed in both E-plane and H-plane. The XPD of this antenna is 28 dB at the boresight. It is seen from Fig. 9 that the XPDs in both E- and H-plane are higher than 26.3 dB over the frequencies 27.2-28.8 GHz and the realized gain is in the range of 6.2-7.2 dBi.

A comparison between the proposed antenna and the corresponding reference antenna without the cross strip is per-

This article has been accepted for publication in a future issue of this journal, but has not been fully edited. Content may change prior to final publication. Citation information: DOI 10.1109/TAP.2020.3017388, IEEE Transactions on Antennas and Propagation

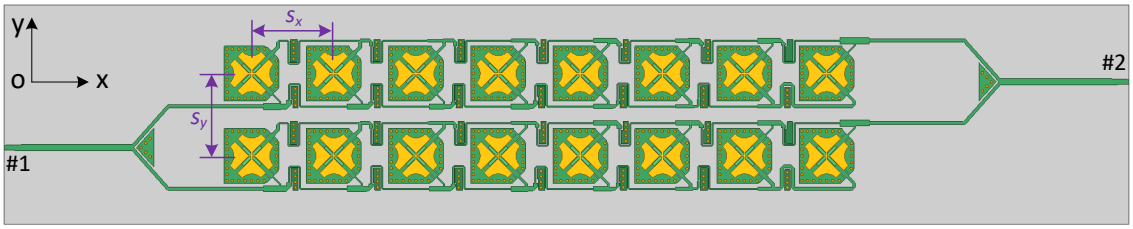

Fig. 12. Geometry of the array antenna. The element spacing in x- and y-direction is $s_x = s_y = 9$ mm and the overall dimension is 123 mm $\times$ 24 mm.

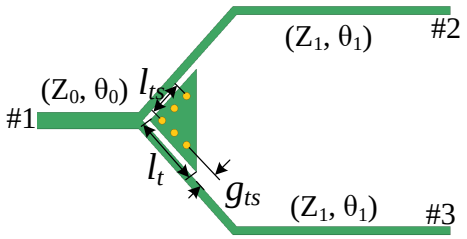

Fig. 13. Layout of the power divider. (Detailed dimensions: $l_{ts} = 1.56$ mm, $l_t = 3.05$ mm, and $g_{ts} = 0.56$ mm.)

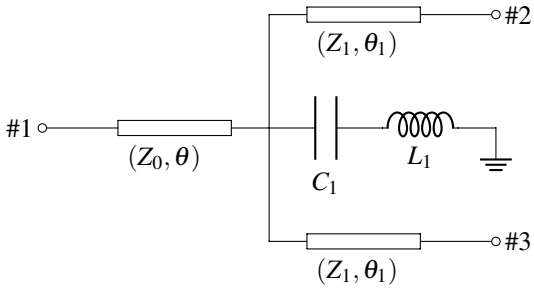

Fig. 14. Circuit representation of the proposed power divider.

formed. Fig. 10 shows the simulated input impedance of the two antennas. It is observed that only one resonance at $f_1 = 28.1$ GHz is found in the reference antenna, even though four parasitic patches are printed on the top surface of Substrate 1. The single resonance comes from the cross slot etched on the ground plane while the added patches produce no additional resonance. The main reason for this is that the coupled patches introduce high capacitance at mmWave frequencies. This effect cannot be mitigated simply by optimizing the size and the gap between the patches. In our design, the cross strip used to unite the separate patches can be equivalent to an inductor between the patches to neutralize the capacitive reactance. As can be seen from Fig. 10, the imaginary part of Z_{in} at the frequencies lower than f_1 moves from negative to zero, and then a new resonance emerges at $f_2 = 27.6$ GHz. The original resonance generated by the cross slot shifts from $f_1 = 28.1$ GHz to $f_3 = 28.4$ GHz. Between the resonance frequency points f_2 and f_3, the imaginary part of Z_{in} almost equals zero and the real part of Z_{in} ranges from 47Ω to 54Ω, indicating that a good impedance matching is achieved.

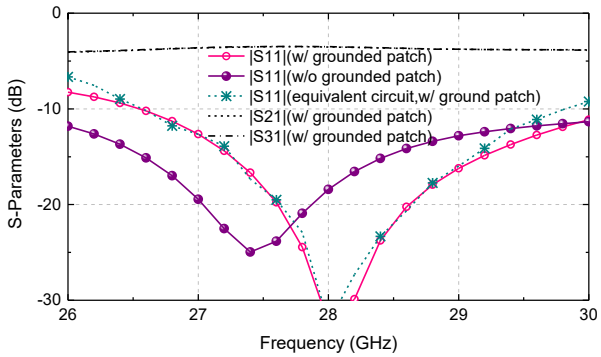

Fig. 15. Simulated S-parameters of the power divider with or without the grounded patch.

The cross strip helps to produce the new resonance. However, the resonance characteristics of the proposed antenna are also affected by the truncated corner size (r_c) and the gap between the patches (w_g). Fig. 11(a) shows the simulated $|S_{11}|$ with different truncated corner sizes. It can be seen that increasing r_c the first resonance frequency shifts to the lower band, while the second resonance frequency almost keeps unchanged. This indicates that the size of the truncated corner only has an effect on the first resonance frequency. In Fig. 11, when increases w_g, the two resonances shift toward the center frequency and merge into one resonance when $w_g = 0.65$ mm. This implies that the gap between patches can affect both resonances and proper selection of w_g can achieve good impedance matching over a wide bandwidth.

III. Antenna Array

A. Configuration

As shown in Fig. 12, a 2×8 dual slant polarized antenna array is designed to exemplify the performance of the proposed antenna element in array antenna design. The antenna element separations in x- and y-direction are $s_x = s_y = 9$ mm ($0.84\lambda_0$). Port #1 and #2 are the feeding ports, of which port #1 is used to excite the antenna array for -45° slant polarization and port #2 is used to excite the antenna array for $+45^\circ$ slant polarization. Each feeding port is followed by an equal power divider. Different from the structure of conventional power dividers, a shorted patch is inserted between the two output branches of the power divider. Two series feeding networks are designed to feed and connect all the antenna elements. In order to realize high compactness, the series

This article has been accepted for publication in a future issue of this journal, but has not been fully edited. Content may change prior to final publication. Citation information: DOI 10.1109/TAP.2020.3017388, IEEE Transactions on Antennas and Propagation

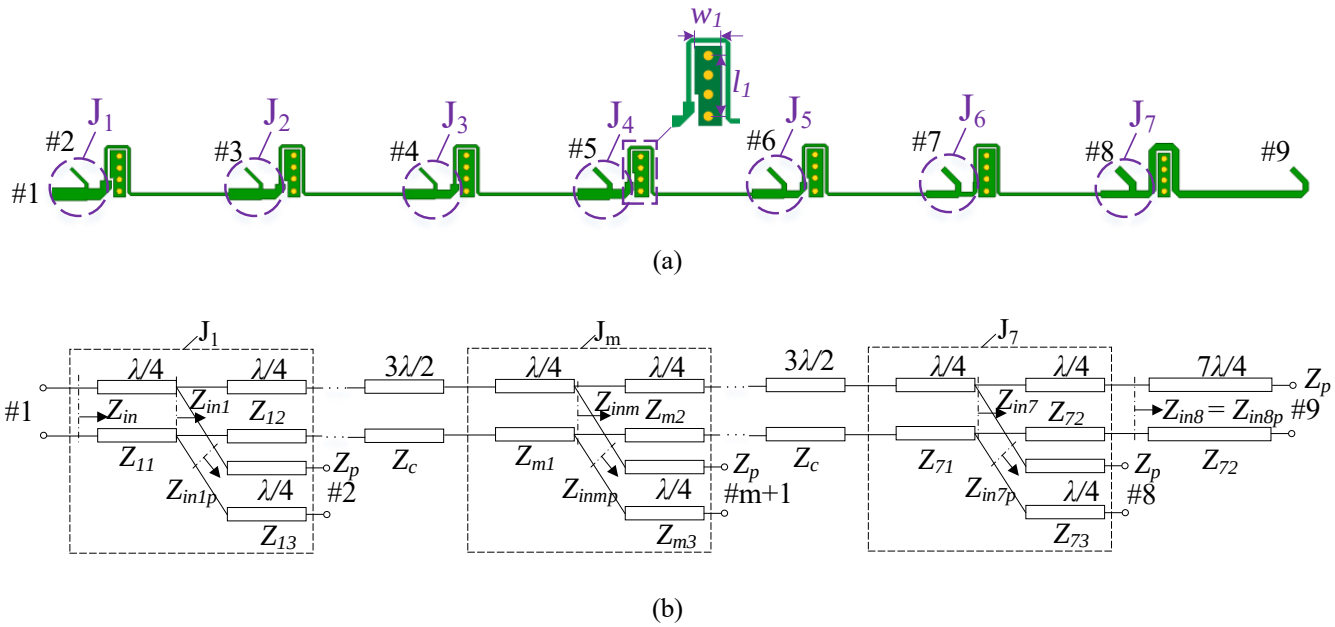

Fig. 16. Series feeding network. (a) Layout. (b) Equivalent circuit.

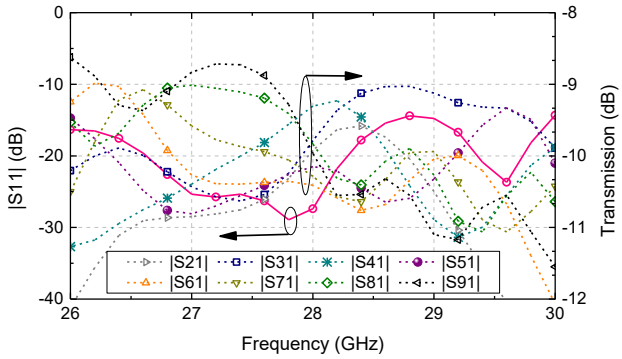

Fig. 17. Simulated $|S_{11}|$ and the transmission coefficients of the designed series feeding network.

feeding networks are interleaved between the linear antenna arrays. Uniform excitation is achieved between the antenna elements by adjusting the impedance of transmission lines. Similar to the power divider design, a shorted patch is added to each bend of the microstrip line to improve the impedance matching. The effect of the shorted patch on the performance will be discussed in the following section.

B. Feeding Network

In this antenna array, the feeding networks include the design of a power divider and a series feeding network. Fig. 13 shows the layout of the designed equal power divider. Ideally, the characteristic impedances of the microstrip lines connected to the input port #1 and the output port #2 or #3 are $Z_0 = 50\Omega$ and $Z_1 = 71\Omega$, respectively; the electric length of the transmission line θ_1 is $\lambda/4$. However, due to the parasitic effect caused by the structure discontinuity at mmWaves, the center operation frequency of the reflection coefficient $|S_{11}|$ would shift to the lower band when designing the power divider by taking these values, as shown in Fig. 15. This parasitic effect cannot be mitigated by adjusting the microstrip impedance or varying the microstrip electric length. In our design, a grounded patch is inserted between the two output branches to alleviate the side effect caused by the discontinuity. The V-shaped shorting vias are used to connect the patch to the ground plane. To better understand its working mechanism, the equivalent circuit model of the proposed power divider is developed and shown in Fig. 14. The grounded patch is modeled as a series *L-C* circuit in which $L_1 = 0.42$ nH and $C_1 = 0.028$ pF. The values of L_1 and C_1 are extracted by carrying out curve-fitting based on the EM simulation results. The series *L-C* circuit is connected to the transmission lines with the characteristic impedance Z_1 and the electric length θ_1 in parallel. The capacitance C_1 is the coupling between the output branch and the grounded patch, and L_1 is the inductance caused by the shorting vias. Thus, the center frequency of S_{11} can be controlled by varying l_{ts}, g_{ts} and l_t as they affect the values of L_1 and C_1. Fig. 15 compares the simulated reflection coefficients $|S_{11}|$ of the proposed power divider and its equivalent circuit representation. The center frequency of $|S_{11}|$ moves from 27.5 GHz to 28 GHz after inserting the shorted patch between the output branches. It is also seen that the transmission coefficients $|S_{21}|$ and $|S_{31}|$of the designed power divider range from –3.4 dB to –3.5 dB over the operation frequency band of the antenna.

The series feeding network is used to feed the antenna elements uniformly, which is designed at the bottom layer of Substrate 2. The layout and its equivalent circuit are shown in Fig. 16. The network mainly includes seven microstrip junctions and each junction has three quarter-wavelength impedance transformers. Port #1 is the feeding port. Port #2 - #9 are output ports which connect to the designed antenna elements with input impedance Z_p. The realization of

This article has been accepted for publication in a future issue of this journal, but has not been fully edited. Content may change prior to final publication. Citation information: DOI 10.1109/TAP.2020.3017388, IEEE Transactions on Antennas and Propagation

TABLE I
IMPEDANCES IN EACH JUNCTION OF THE SERIES FEEDING NETWORK

Junction	Z_{m1} (Ω)	Z_{m2} (Ω)	Z_{m3} (Ω)
J_1	50	53.4	100
J_2	53.4	58	100
J_3	58	63	100
J_4	55	61.2	86.6
J_5	61.2	71	86.6
J_6	71	86.6	86.6
J_7	71	71	71

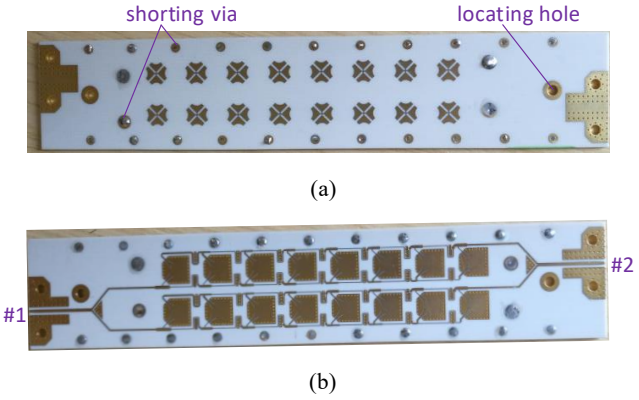

Fig. 18. Fabricated prototype of the designed antenna array. (a) Top view. (b) Bottom view.

such a network is based on its equivalent circuit illustrated in Fig. 16(b), where Z_{m1}, Z_{m2}, $Z_{m3}(m=1,2,...,7)$ are the branch impedances of the m^{th} junction. $Z_{inm}(m=1,2,...,8)$ and $Z_{inmp}(m=1,2,...,7)$ are the input impedances seen from different points. According to the transmission line theory [34], the relationship between these impedances are given by

$$Z_{in7} = Z_{in8p}//Z_{in7p} = (Z_{73}^2/Z_p)//(Z_{72}^2/Z_p) \tag{3}$$

$$Z_{71} = \sqrt{Z_{in7}Z_c} \tag{4}$$

$$Z_{inm} = (Z_{m2}/4Z_p^2)//Z_{inmp} = (Z_{m2}/4Z_p^2)//(Z_{m3}^2/Z_p) \tag{5}$$

$$Z_{m1} = \sqrt{Z_{inm}Z_c}, ..., Z_{11} = \sqrt{Z_{in1}Z_{in}} \tag{6}$$

where the input impedance of the antenna element is $Z_p = 50\Omega$ and the impedance of the transmission line with the length of $3\lambda/2$ is set to $Z_c = 100\Omega$. To avoid microstrips being too narrow or too wide, here the characteristic impedance of each transmission line is specified in the range 50-100Ω. By solving (3)-(6), the branch impedances of all the microstrip junctions are obtained and the values are given in Table I. Due to the discontinuity at each bend of microstrip lines, strong parasitic effect also exists in this series feeding network, which makes the center frequency of reflection coefficient shift to the lower frequency band. Thus, similar to the power divider design, a shorted patch with the dimensions of $l_1 = 1.8$ mm and $w_1 = 0.8$ mm is inserted in each bend. Fig. 17 shows the simulated $|S_{11}|$ and the transmission coefficients of the designed series feeding network. It is observed that $|S_{11}|$ is less than –14 dB from 26 GHz to 30 GHz. The transmission amplitudes vary from –10.5 dB to –9.3 dB at 28 GHz and the amplitude imbalance is ±1.1 dB over the operating frequency

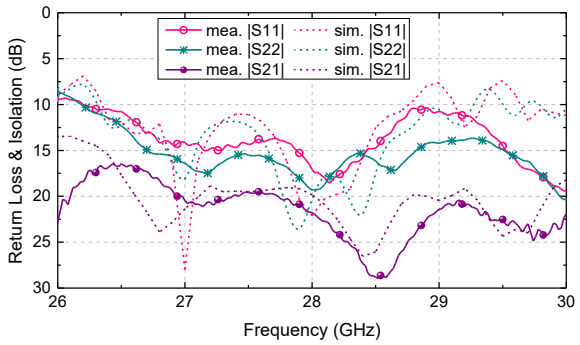

Fig. 19. Simulated and measured S-parameters of the designed array antenna.

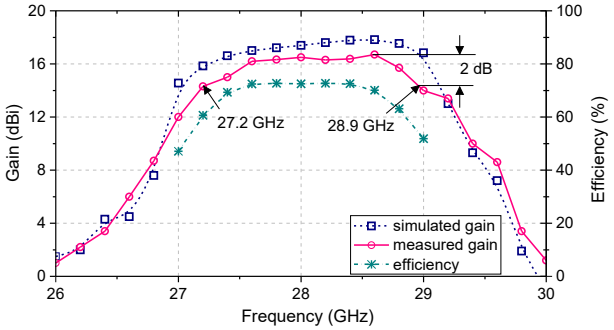

Fig. 20. Gain and efficiency of the proposed antenna array.

27.2-28.8 GHz. This variation is acceptable considering that it is a series network with eight output ports.

IV. EXPERIMENTAL RESULTS

To verify the proposed design, a prototype of the antenna array is fabricated and tested. Fig. 18 shows the top and bottom view of the fabricated antenna. A series of shorting vias located along the laminates are added to make sure that the ground planes of both laminates are well connected. Two locating holes placed near the feeding ports are used for alignment.

A. Antenna Performance

Fig. 19 presents the measured and simulated results of the return loss ($|S_{11}|$) and the isolation ($|S_{21}|$) between port #1 and #2. It is seen that the simulated and measured results agree reasonably well with each other in the frequency band 26-29 GHz. The simulated impedance bandwidth for return loss higher than 10 dB is 26.3–28.8 GHz, which is wider than the operation bandwidth of the antenna element. The bandwidth extension is mainly caused by the propagating loss from the feeding network and incomplete mismatching of the antenna element outside the bandwidth. The measured impedance bandwidth for return loss higher than 10 dB is 26.2-30 GHz. The discrepancy between the measured and the simulated return loss at the upper band 29-30 GHz is due to the misalignment between the two laminate boards. The measured isolation between port #1 and #2 is larger than 23 dB

This article has been accepted for publication in a future issue of this journal, but has not been fully edited. Content may change prior to final publication. Citation information: DOI 10.1109/TAP.2020.3017388, IEEE Transactions on Antennas and Propagation

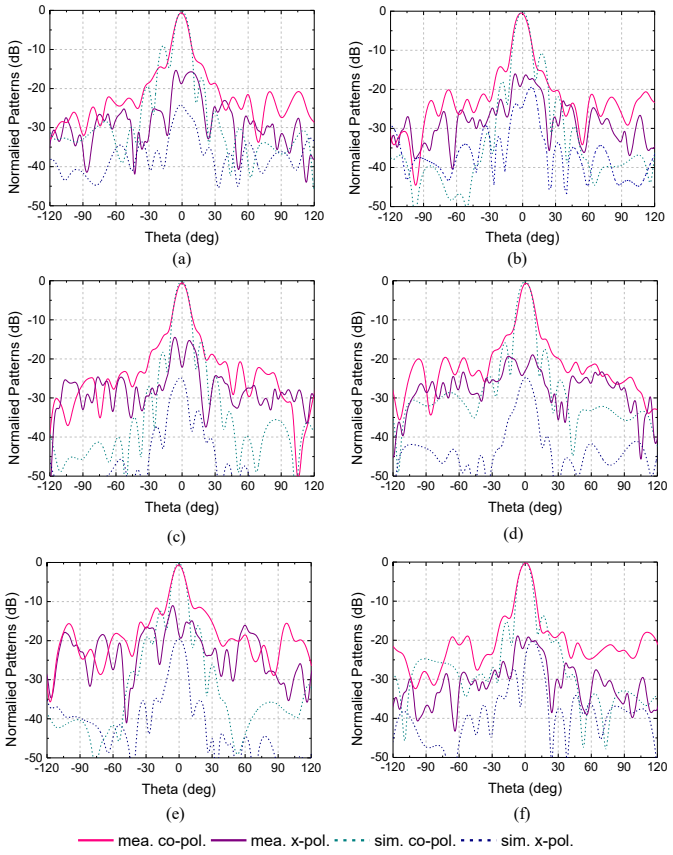

Fig. 21. Normalized far field radiation patterns in the planes of (a) $\varphi = 45^\circ$ at 27.2 GHz, (b) $\varphi = -45^\circ$ at 27.2 GHz, (c) $\varphi = 45^\circ$ at 28 GHz, (d) $\varphi = -45^\circ$ at 28 GHz, (e) $\varphi = 45^\circ$ at 28.8 GHz, and (f) $\varphi = -45^\circ$ at 28.8 GHz.

at 28 GHz and higher than 20 dB over the frequency band of interest, 27.2-28.8 GHz. The simulated and measured realized gain when port #1 is excited is shown in Fig. 20. The measured gain is up to 16.7 dBi, and the bandwidth of the gain 2 dB lower than the peak gain is 27.2-28.9 GHz. Because the losses caused by the connectors are not calibrated, the measured gain is about 0.9 dB smaller than the simulated one. The radiation efficiency calculated from the simulated directivity and gain is up to 75% while decreases to 60% at the edge frequencies, 27.2 GHz and 28.8 GHz.

Fig. 21 shows the measured and simulated far field radiation patterns at 27.2 GHz, 28 GHz and 28.8 GHz. As expected, the co-polarization patterns in both planes, $\varphi = 45^\circ$ and $\varphi = -45^\circ$, are very similar to each other. The measured unidirectional radiation patterns at 28 GHz are observed with side-lobe levels less than –14 dB. The simulated and measured XPD at the boresight is 25 dB. Off the boresight angle, the measured XPD is decreased. In this prototype, the alignment between the laminates is manually performed, where the positioning error would degrade the antenna performance. To characterize the board-to-board misalignment, the relative position between the top and bottom laminate in the y-axis direction (see Fig. 12) is defined as Δd (e.g., the two laminates are perfectly aligned when Δd = 0 mm). Fig. 22 shows the simulated radiation patterns with different Δd. The XPD in both planes of $\varphi = 45^\circ$

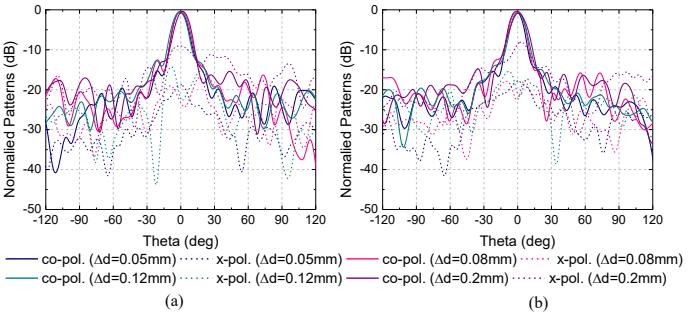

Fig. 22. Simulated normalized far field radiation patterns in the planes of (a) $\varphi = 45^\circ$, and (b) $\varphi = -45^\circ$ at 28 GHz with different board-to-board misalignment Δd.

and $\varphi = -45^\circ$ is degraded with the increase of Δd. It is worth noting that there is a null observed in the cross-polarized radiation patterns at the boresight when Δd is in the range 0.08-0.15 mm. These patterns look similar to the radiation patterns in our measurement. Thus, it can be concluded that the board-to-board misalignment is the main factor resulting in the discrepancies between the simulated and measured results.

B. Comparison and Discussion

A comparison between our work and the reported mmWave antenna arrays with slant polarization is carried out in Table II. Note that the aperture efficiency of an antenna in the table is calculated by [35]

$$\eta_{ap.} = \frac{G_{peak}\lambda_0^2}{4\pi A_{ap}} \tag{7}$$

where G_{peak} and A_{ap} are the peak gain and the physical size of the antenna, respectively. The antenna arrays in [19] and [21] has high aperture efficiency, but they are only able to operate with single slant operation and has high profile. The dual slant polarized antenna arrays in [22], [23] are realized by interleaving their orthogonally polarized antenna elements in separate rows. Thus, they has low aperture efficiency, low XPD and large size. High gain is achieved in the dual slant polarized antenna element reported in [25]. However, this antenna has very large size, resulting in low aperture efficiency and making it not suitable for antenna array design. In comparison, the proposed antenna array is able to work with dual slant polarization while maintaining high XPD, good aperture efficiency, and low profile. In our design, the bandwidth of the gain 2 dB down is 6.0%, which is almost equal to the impedance bandwidth of the antenna element.

V. Conclusion

This paper proposes a novel $\pm 45^\circ$ dual slant polarized antenna operating at 28 GHz. By introducing the corner-fed SIW cavity, high port isolation and XPD are achieved. The operating bandwidth is improved by employing four corner-truncated patches connected with a thin cross strip. A 2×8 array antenna is conceived by using the proposed antenna element to exemplify its performance in array antenna designs. Compared with the traditional single/dual slant polarized mmWave antennas, the proposed antenna exhibits high

TABLE II
COMPARISON BETWEEN THE PROPOSED ANTENNA AND THE REPORTED MMWAVE ANTENNAS WITH 45° SLANT POLARIZATION

Reference	Operation Bandwidth	Polarization	XPD (dB)	$\eta_{ap.}$	h/λ_0	$N_x \times N_y$	Peak Gain (dBi)
[19]	(34-36GHz)/5.7%	single	n.a.	51%	$0.207\lambda_0$	1×8	13.5
[21]	(59-63 GHz)/6.6%	single	18	44%	$5.1\lambda_0$	4×4	17
[22]	(25.7-26.3 GHz)/2.3%	dual	10	22%	$0.017\lambda_0$	6×7	22
[23]	(74.5-82 GHz)/9.3%	dual	16	20%	$0.067\lambda_0$	1×8	15.2
[25]	(56.2-65.4 GHz)/15.3%	dual	n.a.	22%	$0.226\lambda_0$	1×1	12.3
This work	(27.2-28.9 GHz)/6.0%	dual	25	39%	$0.076\lambda_0$	2×8	16.7

XPD, good aperture efficiency, small size, low profile, and low complexity. The proposed antenna would be a promising candidate for mmWave base station applications.

REFERENCES

[1] J. F. Valenzuela-Valdes, M. A. Garcia-Fernandez, A. M. Martinez-Gonzalez, and D. A. Sanchez-Hernandez, "Evaluation of true polarization diversity for MIMO systems," *IEEE Trans. Antennas Propag.*, vol. 57, no. 9, pp. 2746–2755, Sep. 2009.

[2] X. S. Fang, K. W. Leung, and K. M. Luk, "Theory and experiment of three-port polarization-diversity cylindrical dielectric resonator antenna," *IEEE Trans. Antennas Propag.*, vol. 62, no. 10, pp. 4945–4951, Oct. 2014.

[3] W. Lee and Yu Yeh, "Polarization diversity system for mobile radio," *IEEE Trans. Commun.*, vol. 20, no. 5, pp. 912–923, Oct. 1972.

[4] X. Li, X. Huang, Z. Nie, and Y. Zhang, "Equivalent relations between interchannel coupling and antenna polarization coupling in polarization diversity systems," *IEEE Trans. Antennas Propag.*, vol. 55, no. 6, pp. 1709–1715, June 2007.

[5] R. G. Vaughan, "Polarization diversity in mobile communications," *IEEE Transactions on Vehicular Technology*, vol. 39, no. 3, pp. 177–186, Aug. 1990.

[6] B. Lindmark and M. Nilsson, "On the available diversity gain from different dual-polarized antennas," *IEEE J. Sel. Areas Commun.*, vol. 19, no. 2, pp. 287–294, Feb. 2001.

[7] Y. Gou, S. Yang, Q. Zhu, and Z. Nie, "A compact dual-polarized double E-shaped patch antenna with high isolation," *IEEE Trans. Antennas Propag.*, vol. 61, no. 8, pp. 4349–4353, Aug. 2013.

[8] J. Deng, L. Guo, Y. Yin, J. Qiu, and Z. Wu, "Broadband patch antennas fed by novel tuned loop," *IEEE Trans. Antennas Propag.*, vol. 61, no. 4, pp. 2290–2293, April 2013.

[9] B. Q. Wu and K. Luk, "A broadband dual-polarized magneto-electric dipole antenna with simple feeds," *IEEE Antennas Wireless Propag. Lett.*, vol. 8, pp. 60–63, 2009.

[10] M. Barba, "A high-isolation, wideband and dual-linear polarization patch antenna," *IEEE Trans. Antennas Propag.*, vol. 56, no. 5, pp. 1472–1476, May 2008.

[11] L. Wen, S. Gao, Q. Luo, Q. Yang, W. Hu, and Y. Yin, "A low-cost differentially driven dual-polarized patch antenna by using open-loop resonators," *IEEE Trans. Antennas Propag.*, vol. 67, no. 4, pp. 2745–2750, April 2019.

[12] Y. Zhu, Y. Chen, and S. Yang, "Decoupling and low-profile design of dual-band dual-polarized base station antennas using frequency-selective surface," *IEEE Trans. Antennas Propag.*, vol. 67, no. 8, pp. 5272–5281, Aug 2019.

[13] L. Wen, S. Gao, Q. Luo, C. Mao, W. Hu, Y. Yin, Y. Zhou, and Q. Wang, "Compact dual-polarized shared-dipole antennas for base station applications," *IEEE Trans. Antennas Propag.*, vol. 66, no. 12, pp. 6826–6834, Dec 2018.

[14] M. V. Komandla, G. Mishra, and S. K. Sharma, "Investigations on dual slant polarized cavity-backed massive MIMO antenna panel with beamforming," *IEEE Trans. Antennas Propag.*, vol. 65, no. 12, pp. 6794–6799, Dec 2017.

[15] T. Tomura, Y. Miura, M. Zhang, J. Hirokawa, and M. Ando, "A 45° linearly polarized hollow-waveguide corporate-feed slot array antenna in the 60-GHz band," *IEEE Trans. Antennas Propag.*, vol. 60, no. 8, pp. 3640–3646, Aug 2012.

[16] S. Sugawa, K. Sakakibara, N. Kikuma, and H. Hirayama, "Low-sidelobe design of microstrip comb-line antennas using stub-integrated radiating elements in the millimeter-wave band," *IEEE Trans. Antennas Propag.*, vol. 60, no. 10, pp. 4699–4709, Oct 2012.

[17] Y. Yang, B. Sun, G. Zhang, and L. Shen, "TFSIW-excited dual-polarized array antenna with 30 beam-pointing for millimeter-wave applications," *IEEE Trans. Antennas Propag.*, vol. 67, no. 8, pp. 5740–5745, Aug 2019.

[18] B. Liu, R. Zhao, Y. Ma, Z. Guo, X. Wei, W. Xing, and Y. Wang, "A 45° linearly polarized slot array antenna with substrate integrated coaxial line technique," *IEEE Antennas Wireless Propag. Lett.*, vol. 17, no. 2, pp. 339–342, Feb 2018.

[19] M. S. Abdallah, Y. Wang, W. M. Abdel-Wahab, and S. Safavi-Naeini, "Design and optimization of SIW center-fed series rectangular dielectric resonator antenna array with 45 linear polarization," *IEEE Trans. Antennas Propag.*, vol. 66, no. 1, pp. 23–31, Jan 2018.

[20] D. Kim, W. Chung, C. Park, S. Lee, and S. Nam, "A series slot array antenna for 45 °-inclined linear polarization with SIW technology," *IEEE Trans. Antennas Propag.*, vol. 60, no. 4, pp. 1785–1795, April 2012.

[21] A. B. Guntupalli and K. Wu, "45° linearly polarized high-gain antenna array for 60-GHz radio," *IEEE Antennas Wireless Propag. Lett.*, vol. 13, pp. 384–387, 2014.

[22] Sehyun Park, Y. Okajima, J. Hirokawa, and M. Ando, "A slotted post-wall waveguide array with interdigital structure for 45° linear and dual polarization," *IEEE Trans. Antennas Propag.*, vol. 53, no. 9, pp. 2865–2871, Sep. 2005.

[23] Y. Yu, W. Hong, Z. H. Jiang, and H. Zhang, "E-band low-profile, wideband 45° linearly polarized slot-loaded patch and its array for millimeter-wave communications," *IEEE Trans. Antennas Propag.*, vol. 66, no. 8, pp. 4364–4369, Aug 2018.

[24] Y. J. Cheng, X. Y. Bao, and Y. X. Guo, "60-GHz LTCC miniaturized substrate integrated multibeam array antenna with multiple polarizations," *IEEE Trans. Antennas Propag.*, vol. 61, no. 12, pp. 5958–5967, Dec 2013.

[25] S. Liao and Q. Xue, "Dual polarized planar aperture antenna on LTCC for 60-GHz antenna-in-package applications," *IEEE Trans. Antennas Propag.*, vol. 65, no. 1, pp. 63–70, Jan 2017.

[26] R. C. Paryani, P. F. Wahid, and N. Behdad, "A wideband, dual-polarized, substrate-integrated cavity-backed slot antenna," *IEEE Antennas Wireless Propag. Lett.*, vol. 9, pp. 645–648, 2010.

[27] A. Elsherbini, J. Wu, and K. Sarabandi, "Dual polarized wideband directional coupled sectorial loop antennas for radar and mobile base-station applications," *IEEE Trans. Antennas Propag.*, vol. 63, no. 4, pp. 1505–1513, 2015.

[28] J. Hu, Z. Hao, and W. Hong, "Design of a wideband quad-polarization reconfigurable patch antenna array using a stacked structure," *IEEE Trans. Antennas Propag.*, vol. 65, no. 6, pp. 3014–3023, June 2017.

[29] Y. Li and K. Luk, "60-GHz dual-polarized two-dimensional switch-beam wideband antenna array of aperture-coupled magneto-electric dipoles," *IEEE Trans. Antennas Propag.*, vol. 64, no. 2, pp. 554–563, 2016.

[30] S. Mukherjee and A. Biswas, "Substrate integrated waveguide (SIW) cavity backed slot antenna for polarization diversity application," in *2015 IEEE Applied Electromagnetics Conference (AEMC)*, Dec 2015, pp. 1–2.

[31] H. B. Wang and Y. J. Cheng, "Broadband printed-circuit-board characterization using multimode substrate-integrated- waveguide resonator," *IEEE Trans. Antennas Propag.*, vol. 65, no. 6, pp. 2145–2152, June 2017.

[32] Feng Xu and Ke Wu, "Guided-wave and leakage characteristics of substrate integrated waveguide," *IEEE Trans. Antennas Propag.*, vol. 53, no. 1, pp. 66–73, Jan 2005.

[33] R. Garg, K. Gupta, and R. Sharan, "A thin wall leaky waveguide antenna," *IEEE Trans. Antennas Propag.*, vol. 23, no. 1, pp. 107–112, January 1975.

[34] D. Pozar, *Microwave Engineering, 4th ed.* John Wiley & Sons, 2011.

[35] W. L. Stutzman and G. A. Thiele, *Antenna Theory and Design, 3rd ed.* Hoboken, NJ, USA: Wiley, 2012.